CHEMISTRY OF MATERIALS
Article

Chem. Mater. **2010,** *22,* 6117–6124 6117
DOI:10.1021/cm101881b

Synthesis and Characterization of Near-Infrared Cu−In−Se/ZnS Core/Shell Quantum Dots for In vivo Imaging

E. Cassette,[†] T. Pons,*[,†] C. Bouet,[†] M. Helle,[‡] L. Bezdetnaya,[‡] F. Marchal,[‡] and B. Dubertret[†]

[†]*Laboratoire de Physique et Etude des Matériaux, UMR 8213, ESPCI, CNRS, Université Pierre et Marie Curie, 10, rue Vauquelin, 75005 Paris, France, and* [‡]*Centre de Recherche en Automatique de Nancy, Nancy-University, CNRS, Centre Alexis Vautrin, avenue de Bourgogne, 54511 Vandoeuvre-lès-Nancy Cedex, France*

Received July 6, 2010. Revised Manuscript Received September 28, 2010

Near-infrared (NIR) semiconductor quantum dots (QDs) represent promising fluorescent probes for biological and biomedical imaging. $CuInSe_2$ is a good candidate for these applications due to its bandgap in the near-infrared and the reduced toxicity of its components compared to other NIR QD materials (CdTe, CdHgTe, PbS, etc.). Here we present a simple one-pot synthetic route without injection to make fluorescent sphalerite Cu−In−Se core and Cu−In−Se/ZnS core/shell QDs. We show that the photoluminescence (PL) of the resulting core QDs can be tuned from ∼700 nm to ∼1 μm depending on the QD size (from ∼2 to ∼5 nm in diameter). The optical and structural properties of these QDs are consistent with charge recombination via donor−acceptor levels instead of direct excitonic recombination. Finally, we show that the growth of a ZnS shell around these QDs increases their PL quantum yield substantially (up to 40−50% at 800 nm) and allows preservation of their PL properties after solubilization into water and *in vivo*, as demonstrated by detection of the regional lymph node in a mouse.

Semiconductor nanocrystals or quantum dots (QDs) have emerged as a novel class of light-absorbing and -emitting materials for many applications (LEDs, photovoltaics, thin film transistors, etc.) because of their unique electronic and optical properties.[1−3] In addition, their high extinction coefficient, brightness, and photostability make them promising fluorescent probes for biological imaging.[4,5] These diverse and promising applications have triggered considerable progress in the synthesis of core and core−shell QDs composed of many II−VI, IV−VI, and III−V materials (see, for examples, refs 6 and 7 and references therein). Because the bandgap of these particles depends on both their size and composition, these QDs now span a broad wavelength range, from the UV (CdS, ZnSe, etc.) to the infrared (PbS, PbSe, Cd_3P_2, etc.). The near-infrared (NIR) range (∼700−1100 nm) corresponds to a spectral region of minimal absorbance and diffusion by biological tissues and is particularly interesting for *in vivo* fluorescence imaging applications.[8] Near-infrared QDs are therefore promising fluorescent probes for several biomedical applications such as optically guided surgery.[9,10] However, so far applications of QDs to the clinical field have been hampered by the high toxicity of the NIR QD constituents as in CdTe, CdHgTe, and PbS. Other applications of NIR QDs, including photovoltaics, would strongly benefit from the development of less toxic and more environmentally friendly QD materials.

$CuInS_2$ and $CuInSe_2$ are I−III−VI semiconductors with direct bandgaps of 1.53 and 1.04 eV, respectively, and are widely used as thin films in photovoltaic applications.[11−14] There has been recently a renewed interest in the synthesis of $CuInS_2$ and $CuInSe_2$ QDs for *in vivo*

*Corresponding author. E-mail: thomas.pons@espci.fr.

(1) Efros, A. L.; Rosen, M. *Annu. Rev. Mater. Sci.* **2000**, *30*, 475–521.
(2) Murray, C. B.; Kagan, C. R.; Bawendi, M. G. *Annu. Rev. Mater. Sci.* **2000**, *30*, 545–610.
(3) Talapin, D. V.; Lee, J. S.; Kovalenko, M. V.; Shevchenko, E. V. *Chem. Rev.* **2010**, *110*, 389–458.
(4) Medintz, I. L.; Uyeda, H. T.; Goldman, E. R.; Mattoussi, H. *Nat. Mater.* **2005**, *4*, 435–446.
(5) Michalet, X.; Pinaud, F. F.; Bentolila, L. A.; Tsay, J. M.; Doose, S.; Li, J. J.; Sundaresan, G.; Wu, A. M.; Gambhir, S. S.; Weiss, S. *Science* **2005**, *307*, 538–544.
(6) Park, J.; Joo, J.; Kwon, S. G.; Jang, Y.; Hyeon, T. *Angew. Chem., Int. Ed.* **2007**, *46*, 4630–4660.
(7) Reiss, P.; Protiere, M.; Li, L. Small **2009**, *5*, 154−168, and references therein.
(8) Frangioni, J. V. *Curr. Opin. Chem. Biol.* **2003**, *7*, 626–634.
(9) Wu, X.; Liu, H.; Liu, J.; Haley, K. N.; Treadway, J. A.; Larson, J. P.; Ge, N.; Peale, F.; Bruchez, M. P. *Nat. Biotechnol.* **2003**, *21*, 41–46.
(10) Kim, S.; Lim, Y. T.; Soltesz, E. G.; De Grand, A. M.; Lee, J.; Nakayama, A.; Parker, J. A.; Mihaljevic, T.; Laurence, R. G.; Dor, D. M.; et al. *Nat. Biotechnol.* **2004**, *22*, 93–97.
(11) Ramanathan, K.; Contreras, M. A.; Perkins, C. L.; Asher, S.; Hasoon, F. S.; Keane, J.; Young, D.; Romero, M.; Metzger, W.; Noufi, R.; et al. *Prog. Photovoltaics* **2003**, *11*, 225–230.
(12) Klenk, R.; Klaer, J.; Scheer, R.; Lux-Steiner, M. C.; Luck, I.; Meyer, N.; Ruhle, U. *Thin Solid Films* **2005**, *480*, 509–514.
(13) Romeo, A.; Terheggen, A.; Abou-Ras, D.; Batzner, D. L.; Haug, F. J.; Kalin, M.; Rudmann, D.; Tiwari, A. N. *Prog. Photovoltaics* **2004**, *12*, 93–111.
(14) Repins, I.; Contreras, M. A.; Egaas, B.; DeHart, C.; Scharf, J.; Perkins, C. L.; To, B.; Noufi, R. *Prog. Photovoltaics* **2008**, *16*, 235–239.

Published on Web 10/19/2010

imaging or photovoltaics.[15−21] Recent reports have shown in particular that core/shell $CuInS_2$/ZnS QDs may reach reasonably high fluorescence quantum yields in the visible and NIR range, up to ∼800−850 nm, and offer promising alternatives to II−VI QDs for in vivo fluorescence imaging because of the absence of heavily toxic and/or carcinogenic Cd, Pb and Hg metal ions.[17,19,22] We have recently shown that $CuInS_2$/ZnS QDs present a much reduced toxicity compared to CdTeSe/CdZnS core/shell QDs.[22] $CuInSe_2$ QDs could also constitute promising probes for in vivo imaging. In particular, they could reach longer wavelengths (theoretically up to ∼1200 nm) and so allow both excitation and emission processes to occur in an optimal wavelength range (∼800−950 nm). Moreover, the toxicity of their components is reduced compared to cadmium, lead, and mercury. There have been relatively few reports on $CuInSe_2$ QD synthesis, and most of them did not report any photoluminescence (PL).[16,20,23−26] Recently, Nose et al. reported $CuInSe_2$ QDs emitting between 820 and 940 nm but with PL quantum yields (QY) less than 5%.[21] Allen et al. reported the synthesis of Cu−In−Se QDs with PL QY up to 25%.[18] However, the latter QDs could not maintain their PL properties in water due to the lack of a high bandgap shell to protect the Cu−In−Se cores, and the synthesis involved expensive and hazardous bis(trimethylsilyl)-selenide precursor. In this manuscript we report a simple synthetic scheme without injection using selenourea as a selenium precursor, which yields Cu−In−Se core and Cu−In−Se/ZnS core/shell materials emitting from ∼700 nm to ∼1040 nm. We characterize their photophysical and structural properties, discuss the origin of their photoluminescence and demonstrate their application for biological *in vivo* imaging.

Experimental Section

Chemicals. Tri-n-octylphosphine (CYTOP-380, TOP) was a gift from CYTEC. Di-n-octylamine (98%, DOA) was purchased from Acros Organics. Seleneourea was purchased from Strem Chemicals (>99%, SeU). Oleylamine (>70%, OAm), 1-octadecene (90%, ODE), 1-dodecanethiol (>97%, DDT), copper(I) chloride (>99%, CuCl), indium(III) chloride (99.999%, $InCl_3$), zinc chloride (98%, $ZnCl_2$) and potassium ethylxanthogenate (>98%, K(EtX)) were purchased from Sigma-Aldrich. Zinc nitrate hexahydrate (>98%, $Zn(NO_3)_2$ 6 H_2O) and sodium oleate (>82%, Na(OA)) were purchased from Riedel-de Heën. All chemicals were used as provided without further purification. TOP, $InCl_3$, and SeU were stored under an Ar atmosphere, and SeU was additionally kept in the dark.

Cu−In−Se QD Synthesis. In a typical core synthesis, all precursors (0.4 mmol CuCl, 0.4 mmol $InCl_3$, 0.8 mmol SeU) were introduced in a three-necked flask with 10 mL of ODE and 4 mL of TOP and briefly sonicated. Then, 4 mL of OAm and 2 mL of DDT were added. The solution was stirred and degassed for 30 min under vacuum. The flask was then refilled with argon and the solution heated to final temperatures T_f ranging from 80 to 250 °C. Heating was stopped immediately after the target temperature was reached and the flask was cooled down to room temperature. The QDs were precipitated in ethanol (acetone may be added typically up to 5% to avoid phase separation) and centrifuged. Cu−In−Se cores were then redispersed in a nonpolar solvent, typically in 10 mL of hexane.

ZnS Precursor Preparation. Zinc bis(ethylxanthogenate) ($Zn(EtX)_2$) was prepared from K(EtX) and $ZnCl_2$ as follows: 10 mmol of $ZnCl_2$ and 20 mmol of K(EtX) were separately dissolved in 20 mL of distilled water. The solutions were slowly mixed under stirring to form a white precipitate that was isolated, washed for several cycles with water, and dried. $Zn(OA)_2$ was prepared from $Zn(NO_3)_2$ and Na(OA): 15 mmol of $Zn(NO_3)_2$ dissolved in 40 mL of methanol were added to a solution of 30 mmol of Na(OA) dissolved in 200 mL of methanol. The resulting white precipitate was isolated, washed, and dried.

Cu−In−Se/ZnS Core/Shell QD Synthesis. Half of the $CuInSe_2$ cores prepared as indicated above were redispersed in 4 mL of ODE and 1 mL of OAm into a new three-neck flask. The flask was degassed under vacuum at room temperature to remove hexane and H_2O traces. A solution of $Zn(EtX)_2$ and $Zn(OA)_2$ (respectively 40 and 500 mg) dispersed in ODE (2 mL), TOP (3 mL), and DOA (1 mL) was loaded into an injection syringe. One milliliter of this solution was introduced at room temperature into the flask, and the temperature was raised to 190 °C. The rest of ZnS precursors were added dropwise into the flask in 1 h under argon atmosphere. The reaction flask was cooled down at the end of the injection. The resulting Cu−In−Se/ZnS QDs were precipitated in ethanol and acetone and redispersed in hexane.

Optical Characterization. All optical measurements were performed at room temperature with QDs dispersed in hexane or water. Absorption measurements were carried out with a Cary 5E UV−vis-NIR spectrophotometer (Varian). Photoluminescence (PL), photoluminescence excitation (PLE), integrated photoluminescence excitation (IPLE) spectra and time-resolved fluorescence were acquired using a FCS900 spectrometer (Edinburgh Instruments) equipped with R928-P and R5509−72 photomultipliers (Hamamatsu) and a USB2000 fluorimeter (Ocean Optics). PLE and IPLE spectra of QD solutions with optical densities below 0.1 at 300 nm were recorded using excitation wavelengths ranging from 300 to 800 nm. Each PL spectra was normalized by the excitation intensity and then integrated over all emission wavelengths. This integrated intensity was plotted versus the excitation wavelength to provide the IPLE spectrum. The sample fluorescence quantum yields were evaluated in comparison with rhodamine 6G in ethanol as reference (excited at 530 nm) or Indocyanine Green in dimethylsulfoxide for NIR samples (excited at 750 nm).

(15) Panthani, M. G.; Akhavan, V.; Goodfellow, B.; Schmidtke, J. P.; Dunn, L.; Dodabalapur, A.; Barbara, P. F.; Korgel, B. A. *J. Am. Chem. Soc.* **2008**, *130*, 16770–16777.
(16) Guo, Q.; Kim, S. J.; Kar, M.; Shafarman, W. N.; Birkmire, R. W.; Stach, E. A.; Agrawal, R.; Hillhouse, H. W. *Nano Lett.* **2008**, *8*, 2982–2987.
(17) Xie, R.; Rutherford, M.; Peng, X. *J. Am. Chem. Soc.* **2009**, *131*, 5691–5697.
(18) Allen, P. M.; Bawendi, M. G. *J. Am. Chem. Soc.* **2008**, *130*, 9240–9241.
(19) Li, L.; Daou, T. J.; Texier, I.; Kim Chi, T. T.; Liem, N. Q.; Reiss, P. *Chem. Mater.* **2009**, *21*, 2422–2429.
(20) Koo, B.; Patel, R. N.; Korgel, B. A. *J. Am. Chem. Soc.* **2009**, *131*, 3134–3135.
(21) Nose, K.; Omata, T.; Otsuka-Yao-Matsuo, S. *J. Phys. Chem. C* **2009**, *113*, 3455–3460.
(22) Pons, T.; Pic, E.; Lequeux, N.; Cassette, E.; Bezdetnaya, L.; Guillemin, F. o.; Marchal, F. d. r.; Dubertret, B. *ACS Nano* **2010**, *4*, 2531–2538.
(23) Castro, S. L.; Bailey, S. G.; Raffaelle, R. P.; Banger, K. K.; Hepp, A. F. *Chem. Mater.* **2003**, *15*, 3142–3147.
(24) Tang, J.; Hinds, S.; Kelley, S. O.; Sargent, E. H. *Chem. Mater.* **2008**, *20*, 6906–6910.
(25) Zhong, H. Z.; Li, Y. C.; Ye, M. F.; Zhu, Z. Z. *Nanotechnology* **2007**, *18*, 025602.
(26) Norako, M. E.; Brutchey, R. L. *Chem. Mater.* **2010**, *22*, 1613–1615.

Structural Characterization. For the following characterizations, QDs were washed by several cycles of precipitation/redispersion with ethanol and acetone to remove excess organic components. High resolution transmission electron microscopy (HRTEM) images were acquired on a JEOL 2010 field electron gun microscope operated at 200 keV. Elemental analysis was performed by energy-dispersive X-ray spectroscopy (EDX) on a Hitachi S-3600N scanning electron microscope operated at 20 keV. Powder X-ray diffraction (XRD) patterns were acquired using a Philips X'Pert diffractometer with a Cu K_α source. The widths of the XRD peaks are related to the crystallite size by the Scherrer formula

$$\mathrm{FWHM} = \frac{0.89\lambda_{\mathrm{Cu}K\alpha}}{d\cos(\theta)}$$

where fwhm is the full width half-maximum of the peak, $\lambda_{\mathrm{CuK}\alpha}$ is the wavelength of the Cu K_α X-ray source, d is the average crystallite size. and θ is the diffraction angle.

Solubilization in Water. Cu−In−Se/ZnS QDs were precipitated in ethanol and resuspended in chloroform before cap exchange with dithiol sulfobetaine zwitterionic ligands in a water/chloroform biphasic solution as previously described.[27] The resulting QDs were purified by ultrafiltration (Vivaspin, 10 kDa cutoff) and ultracentrifugation on 10−40% sucrose gradients for 20 min on a Optima-Max Beckman-Coulter ultracentrifuge (MLS-50 rotor, 50,000 rpm). The QD band was extracted, purified by ultrafiltration and finally resuspended in 20 mM NaCl aqueous solution.

Small Animal Imaging. Three 10-week-old female Balb/c mice (Balb/cOlaHsd) (Harlan, Gannat, France) weighing 20 g were used in these experiments. Mice were kept in 12 h light/dark cycle and had access to food and water ad libitum. Specific purified diet (TD.94045, Harlan Teklad, Madison, WI, USA) was used to reduce tissue autofluorescence in the NIR spectral region. The animals received care in accordance with established guidelines of FELASA (Federation of European Laboratory Animal Science Associations) and animal procedures were performed in compliance with institutional and national guidelines. The injections were performed under gaseous anesthesia with isoflurane (Forene, Abbott France, Rungis, France) by introducing the mice into a chamber where the air flow with 4.5% of isoflurane was adjusted to 500 mL/min. The anesthesia was maintained by placing the mice under a mask with 2.5% of isoflurane and the air flow of 250 mL/min. Mice were injected subcutaneously (s.c.) in the distal part of the right anterior paw with 20 μL of a solution of $\sim$ 800 nm emitting Cu-In-Se/ZnS QDs ($\sim$0.5 optical density at 690 nm) in phosphate buffer saline (PBS). After product delivery, the right paw was kneaded to improve product migration. *In vivo* optical imaging of QDs was performed using a Fluobeam 700 NIR imaging system (Fluoptics, Grenoble, France). This system is composed of a laser emitting at 690 nm, a 750 nm long-pass emission filter and a CCD camera. The power density of laser irradiation on tissue was 7 mW/cm^2 and the CCD exposure time was 10 ms. The region of interest (ROI) was depilated using a commercial hair-removal cream before imaging. The QD injection point was hidden to improve the visualization of the lymph node.

ICP-MS Measurements. The right axillary lymph node was dissected at four hours post injection and dissolved with 70% HNO_3 under heating. Its concentration in indium was measured by inductively coupled plasma-mass spectrometry (ICP-MS, Laboratoire Ascal, France) and compared with the QD injection solution to determine the injected dose percentage (%ID) in this lymph node.

(27) Muro, E.; Pons, T.; Lequeux, N.; Fragola, A.; Sanson, N.; Lenkei, Z.; Dubertret, B. *J. Am. Chem. Soc.* **2010**, *132*, 4556–4557.

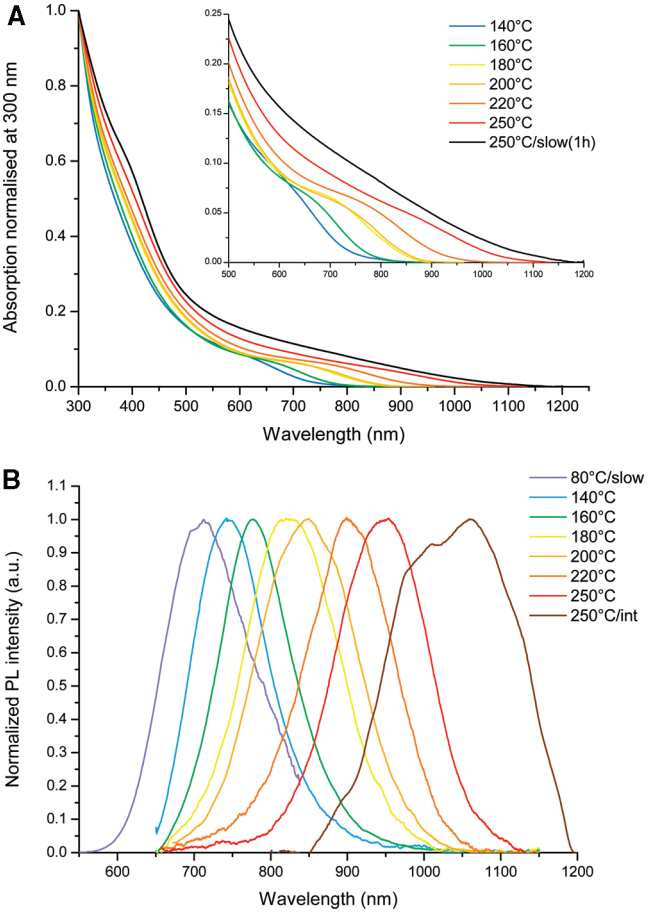

Figure 1. (A) Absorption spectra and (B) PL spectra of Cu−In−Se core QDs. Samples were synthesized by fast heating (T_f = 140−250 °C), slower heating to T_f = 80 °C (B, purple) or T_f = 250 °C with a 1 h rise (A, black), and intermediate heating to T_f = 250 °C (B, brown).

Results and Discussion

Cu−In−Se Core Synthesis. The Cu−In−Se cores were synthesized in a one-pot route without injection. Copper and indium chlorides were solubilized in ODE using TOP, OAm and DDT ligands, and mixed with selenourea in proportions corresponding to $CuInSe_2$ stoichiometry. After degassing, the solution was heated under argon. We tested different types of heating conditions, either "fast" heating, where the final temperature (T_f) is reached in about 10−15 min, or "slow" heating, where the final temperature is reached in about 1 h. Above 40−50 °C, the solution turns limpid and colorless, indicating the complexation of metal chlorides by TOP and SeU dissolution. The solution turns yellow then red at around 110−130 °C for fast heating or starting at 80 °C for slow heating, indicating nanocrystal nucleation. As the temperature increases, the solution turns darker. This synthesis is somewhat similar to the one recently reported by Koo et al.[20] which does not produce fluorescent QDs. This is due to several notable differences: here, selenourea was added directly to the flask instead of being separately

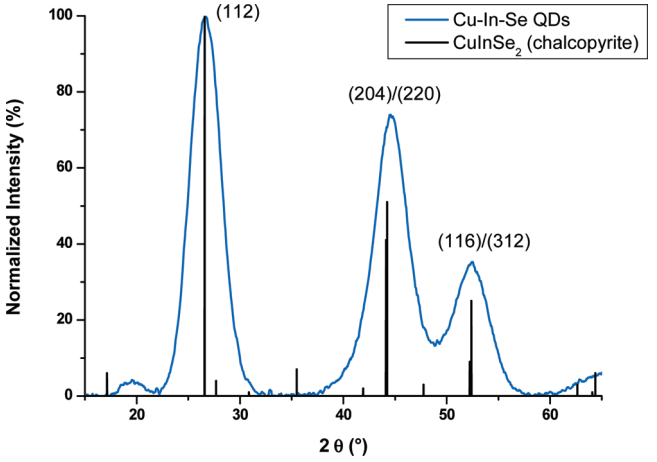

Figure 2. X-ray diffractograms of Cu−In−Se cores synthesized at 160 °C and reference (bulk $CuInSe_2$ chalcopyrite[41]).

dissolved in OAm. We note that absence of OAm in the reaction led to slow nucleation and rapid aggregation of the resulting materials. Another difference is the presence of TOP: in the absence of TOP, QDs were formed but did not show any fluorescence. Finally, we noted that the presence of DDT increased the colloidal stability of the QDs in particular at high temperatures: without DDT, the QDs were unstable above 200 °C. In comparison, the QD reaction solution with DDT could be heated to 250 °C without QD precipitation, which we attribute to stronger binding of DDT ligands compared to OAm or TOP, and this allowed us to reach longer wavelengths.

We will now discuss the optical and structural properties of the obtained Cu−In−Se QDs and the origin of their photoluminescence. The obtained nanocrystals showed absorption and photoluminescence spectra that are dependent on the final temperature T_f (Figure 1A, B). Absorption spectra shifted to redder wavelengths with increasing temperature. PL spectra from fast heating syntheses ranged from 750 nm for T_f = 140 °C to ∼950 nm for T_f = 250 °C. PL quantum yields increase from ∼4% for T_f = 140 °C up to ∼20% for T_f = 180 °C and fall down for redder wavelengths to ∼3% for the sample synthesized at T_f = 250 °C with an intermediate heating (∼20 min). We observed that the optical properties of the Cu−In−Se nanocrystals only evolved very slowly with time when kept at the final temperature for T_f > 100 °C. Slower heating syntheses induced a nucleation at lower temperatures (∼80 °C) and redder wavelengths than fast heating syntheses for the same final temperatures, Figure 1A. Quantum dots synthesized at 250 °C with a one hour temperature rise were non fluorescent, but intermediate heating speed (15−20 min) gave PL emission >1040 nm. In contrast to II−VI QDs, the resulting QD absorption spectra do not display any sharp absorption features, and the PL spectra were broad, typically 110−150 nm fwhm, consistently with what was previously reported for $CuInS_2$ and $CuInSe_2$ QDs.[17−19,21,22] Here we will try to determine whether these optical properties are due to some dispersion in size, shape, and/or composition of the resulting nanoparticles, or to intrinsic optical properties, by examining the QD structural properties.

XRD patterns for fast and intermediate synthesis samples were consistent with $CuInSe_2$ sphalerite (zinc blende) structure (Figure 2) with three major peaks at (26.70 ± 0.04)°, (44.59 ± 0.05)°, and (52.53 ± 0.12)° for the (112), (220), and (312) lattice planes, respectively. We noted the absence of any significant diffraction peak at 35.48° in contrast to the chalcopyrite structure reported with other synthetic procedures.[16,18] This suggests that the indium and copper cations are not ordered in the crystal structure. Similar synthetic conditions using copper iodide and indium acetate reacted with DDT in absence of selenourea yielded $CuInS_2$ QDs.[19] We therefore investigated whether our QDs are composed of pure Cu−In−Se or of a Cu−In−Se/Cu−In−S alloy. The presence of sulfur would cause a shift of the XRD peaks toward those of $CuInS_2$ (the lattice parameter difference between these two materials is about 5%). Here the positions of the diffraction peaks suggest that the QDs do not contain a significant fraction of sulfur atoms for all fast heating samples. In contrast, the S/Se ratio for the sample synthesized by slow heating to 250 °C (1 h temperature rise) was not negligible (estimated to ∼30% with a linear approximation between the peak positions of $CuInSe_2$ and $CuInS_2$ materials) since the XRD peaks were shifted to 27, 44.9, and 53.2° for (112), (220), and (312) lattice planes, respectively. This may be due to a higher depletion of selenourea precursors as the reaction yield increases.

High-resolution transmission electron microscopy (HRTEM) of samples synthesized by fast and intermediate heating showed monocrystalline particles ranging from nearly spherical ∼3 nm QDs for T_f = 180 °C to slightly faceted ∼5 nm (triangular) QDs for T_f = 250 °C (see the Supporting Information, Figure S1). Synthesis at 250 °C with a slow heating (1 h temperature rise) gave both faceted and round NCs larger than 8 nm that were not fluorescent (see the Supporting Information, Figure S1). However, for particles smaller than 5 nm, the low contrast offered by the QDs did not allow accurate determination of their size. We therefore used the Scherrer formula to estimate the size of the Cu−In−Se core QDs from the XRD peak widths. The resulting XRD sizes were well correlated with TEM sizes but were slightly smaller for the sample synthesized with a slow heating to 250 °C (1 h temperature rise, see the Supporting Information, Figure S2). Broadening of the XRD peaks for this specific sample could be attributed to strain and/or composition heterogeneity as indicated by the incorporation of S discussed above. However, XRD size estimation measurements of our Cu−In−Se QDs showed that all QDs were smaller than the bulk exciton of $CuInSe_2$ ($2a_B$ = 10.8 nm), and that the size progressively increases with the reaction temperature (see the Supporting Information, Figure S2). This is consistent with the observed progressive red shift of the QDs due to confinement effects.

To examine the effect of size on the bandgap of these Cu−In−Se QDs, we represented the energy corresponding to the effective bandgap derived from absorption

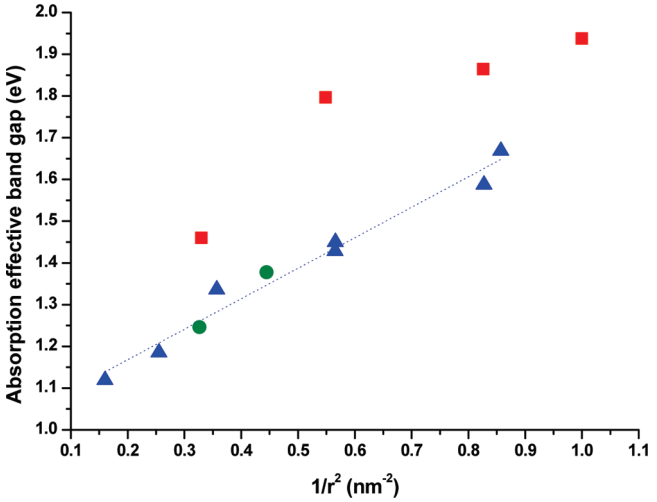

Figure 3. Effective bandgap was plotted versus the inverse square radii of QDs (blue triangles; black line, linear fit). Two other experimental results are shown in red ($CuIn_5Se_8$) and in green ($CuIn_{2.3}Se_4$) from previously reported data[18] for comparison.

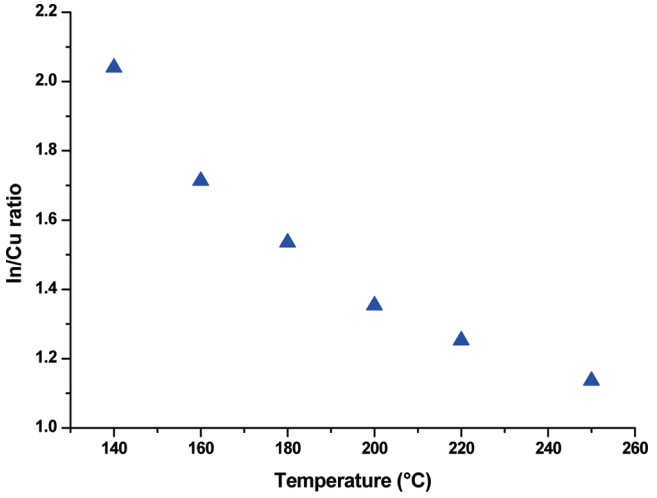

Figure 4. Evolution of the In/Cu ratio in Cu−In−Se core QDs during the fast heating synthesis.

spectra (see the Supporting Information, Figure S3) as a function of the inverse of the QD square diameter (Figure 3, blue triangles). This shows that the effective bandgap energy varies approximately linearly with $1/r^2$, as expected from a simple excitonic confinement model. Extrapolating this curve to infinite size gives a bandgap value of 1.02 ± 0.03 eV, which is comparable to the value of bulk $CuInSe_2$. These data are well-correlated with those reported by Allen et al.[18] for $CuIn_{2.3}Se_4$ QDs, as shown in Figure 3 (green dots). In contrast, the $CuIn_5Se_8$ samples give higher bandgap in particular for smaller QDs (Figure 3, red squares). This may be attributed to the larger difference in composition between these latter QDs and ours (see below), and the corresponding differences in the bulk bandgap and the quantum confinement contribution (carrier effective masses, etc.).

To evaluate the effect of the composition on the sample bandgaps and PL emissions, we studied the In/Cu ratio for fluorescent samples. The composition of the QDs was estimated by EDX spectroscopy and confirmed the presence

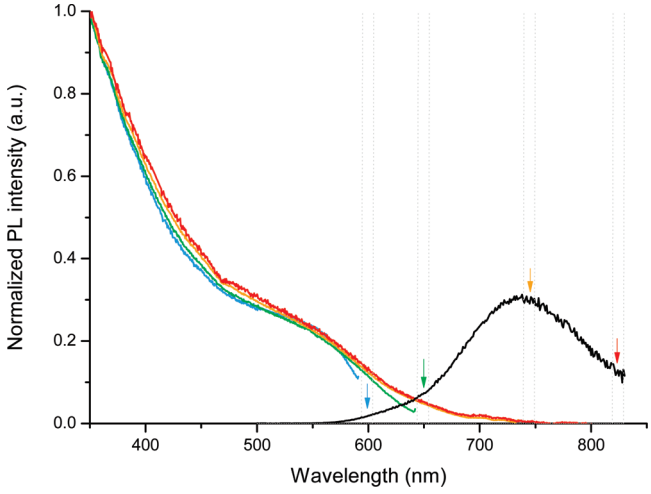

Figure 5. Photoluminescence excitation spectra corresponding to different emission wavelengths (colored arrows) from 600 to 820 nm, and the corresponding PL spectrum excited at 350 nm (black).

of Cu, In, Se in diverse proportions (see the Supporting Information, Table ST1). The spectra also showed the presence of sulfur atoms (S/Se ~30%) for all samples obtained by fast heating. As discussed above in XRD measurements, the sulfur was not incorporated into the QD cores in a significant fraction, suggesting that the DDT ligands participate in the QD surface passivation. The cation/anion proportions were as expected consistent with degrees of oxidation of Cu^+, In^{3+}, and Se^{2-}. The In/Cu ratio in the QDs varies during the synthesis: the initial QDs are rich in indium (In/Cu = ~2 for QDs emitting at λ_{em} = 750 nm) and progressively reaches In/Cu stoichiometry for larger QDs (Figure 4). Many different compositions exist for Cu−In−Se crystals ($CuInSe_2$, $CuIn_{1.5}Se_3$, $CuIn_{2.3}Se_4$, $CuIn_3Se_5$, $CuIn_5Se_8$, etc.), which reflects the high stability of defect pairs: 2 copper vacancies with a substitution of indium on a copper site ($2V_{Cu}^- + In_{Cu}^{2+}$).[28] These materials exhibit very close lattice parameters so the resulting XRD patterns are not distinguishable within our peak widths. To understand the variations of QD composition during the fast heating synthesis, we estimated the In/Cu ratio of the atoms deposited on the QDs between the first sample taken at 140 °C and subsequent reaction times/temperatures using the In, Cu, Se composition and the size of the different QD samples (see the Supporting Information). The In/Cu ratio of the deposited material is close to one at all times (see the Supporting Information, Figure S4). This suggests that the QDs initially nucleate with a high In/Cu ratio and that the subsequent growth corresponds to deposition of stoichiometric $CuInSe_2$. Even though the QD bandgap depends on the composition (the bulk bandgap of $CuInSe_2$ is 1.04 eV, whereas that of $CuIn_3Se_5$ is 1.21 eV,[29]), our results suggest that the shifts in absorption and emission spectra during the synthesis are mainly due to a progressive increase in size resulting in a decrease of quantum confinement effects, and to a lesser extent to a difference in composition.

(28) Zhang, S. B.; Wei, S. H.; Zunger, A.; Katayama-Yoshida, H. *Phys. Rev. B* **1998**, *57*, 9642–9656.
(29) Wasim, S. M.; Rincon, C.; Marin, G.; Delgado, J. M. *Appl. Phys. Lett.* **2000**, *77*, 94–96.

These structural properties provide a framework to better understand the optical properties of our Cu−In−Se QDs. Cu−In−Se PL spectra are broad even for smaller QDs (fwhm ∼110−150 nm) and exhibit large Stokes shifts (from ∼130 to ∼100 nm with increasing wavelength) compared to II−VI QDs, as was previously reported for $CuInS_2$ and $CuInSe_2$.[17−19] In addition, we noted that photoluminescence excitation (PLE) spectra do not vary much with the selected emission wavelength within a QD population (Figure 5). This indicates that QDs with nearly identical absorption properties exhibit very different Stokes shift and emission spectra, in contrast to what is observed with II−VI QDs. So the broad PL spectra may not be attributed only to size and/or composition heterogeneity but must arise from the nature of the PL emission. The PL decay of these Cu−In−Se QDs is dominated by a decay time that is much longer than what is usually observed for II−VI materials (see the Supporting Information, Figure S5A): 170−275 ns compared to ∼10−20 ns for CdSe QDs.[30] These results are also inconsistent with a photoluminescence produced by band-edge exciton recombination. They instead suggest that the exciton energy is rapidly transferred to defect levels within the bandgap, and that the radiative recombination then occurs as a donor−acceptor transition. These donor−acceptor pairs may be linked to the observed presence of $(2V_{Cu}^{-} + In_{Cu}^{2+})$ defect pairs, as discussed above and as previously discussed in other reports.[21] Even though the emission is not directly due to band edge recombination, the PL spectra still shift to the blue when the particle size decreases due to quantum confinement, albeit slower than the absorption spectra (see the Supporting Information, Figure S6). This indicates that the energy of the donor and acceptor electronic levels involved in the radiative recombination are correlated with the energy of the valence and conduction bands.

The PL quantum yield of our Cu−In−Se core QDs was still sensitive to surface oxidation. In particular, transfer of the Cu−In−Se QDs into water by ligand exchange resulted in an immediate loss of the QD PL. It was therefore necessary to grow a high bandgap ZnS shell around the cores to protect them from their environment.

Cu−In−Se/ZnS Core/Shell Synthesis and *In vivo* Imaging. Zinc sulfide was chosen to overcoat the $CuInSe_2$ QDs for its large bandgap (3.61 eV), which provides a type I band alignment[31,32] with Cu−In−Se cores and its relatively close crystalline structure (zinc-blende). The lattice mismatch between ZnS and $CuInSe_2$ is about 7%, which should allow epitaxial growth of several ZnS monolayers without introducing excessive strain on the cores.[33] ZnS presents a reduced toxicity, which is crucial for a surface material that will be in contact with biological tissues.

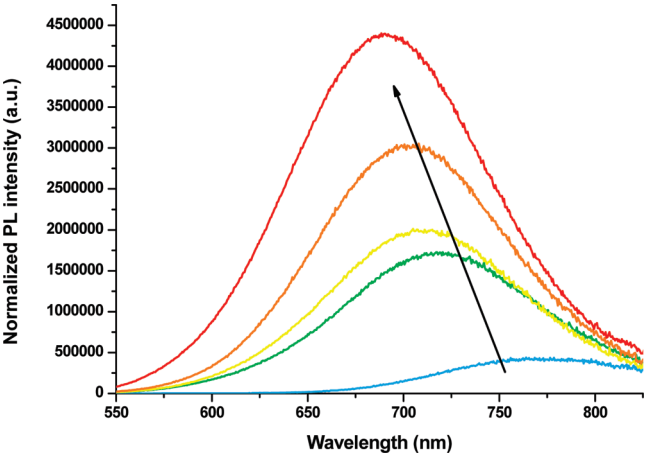

Figure 6. Photoluminescence spectra of Cu−In−Se (blue) and Cu−In−Se/ZnS QDs normalized by their optical density at the excitation wavelength (530 nm), during the growth of a ZnS shell on cores synthesized at 140 °C (from green to red, corresponding to injected volumes of ZnS solution of 0.5, 1, 3, and 4 mL).

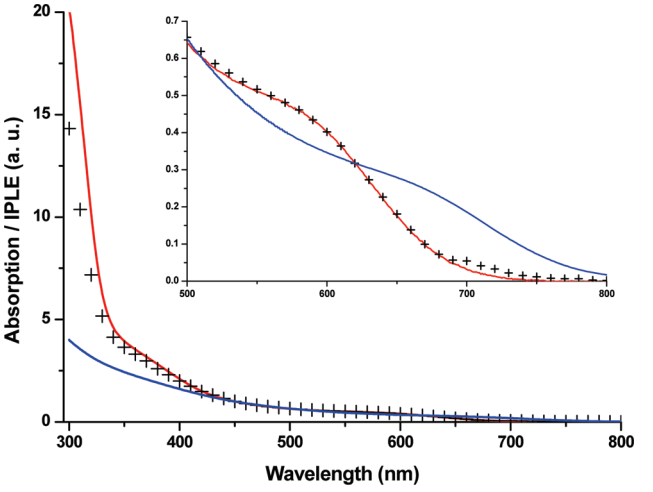

Figure 7. Normalized absorption (red line) and IPLE (crosses) spectra of a core−shell sample after the ZnS shell growth. The absorption spectrum of the corresponding Cu−In−Se cores (T_f = 140 °C) is shown in blue. Inset: zoom.

Moreover, this material is well-resistant to oxidation. Several methods have been developed to grow ZnS shell on QDs, e.g., CdSe, CdS, and more recently, InP[7] or $CuInS_2$.[17,19,22] Here ZnS shell growth was performed by dropwise injection of zinc bis(ethylxanthogenate) and zinc oleate at 190 °C.[34] The high reactivity of these precursors allows using a relatively low reaction temperature and avoids interdiffusion of Zn into the cores and excessive dissolution of the Cu−In−Se cores with OAm.

For all samples, the fluorescence quantum yield was strongly enhanced during the growth of ZnS. For example, for cores synthesized at 140 °C, ZnS shell growth resulted in a QY increasing about 10-fold, from ∼4 to 43% as shown in Figure 6, which is to the best of our knowledge the highest PL QY reported for Cu−In−Se QDs. This may indicate an improved surface passivation of the core by ZnS. We found that under excitation, the

(30) Crooker, S. A.; Barrick, T.; Hollingsworth, J. A.; Klimov, V. I. *Appl. Phys. Lett.* **2003**, *82*, 2793–2795.
(31) Nakada, T.; Hongo, M.; Hayashi, E. *Thin Solid Films* **2003**, *431*, 242–248.
(32) Worz, M.; Pschorr-Schoberer, E.; Flierl, R.; Preis, H.; Gebhardt, W. *J. Appl. Phys.* **1998**, *84*, 2871–2875.
(33) Ithurria, S.; Guyot-Sionnest, P.; Mahler, B.; Dubertret, B. *Phys. Rev. Lett.* **2007**, *99*, 265501.
(34) Protiere, M.; Reiss, P. *Nanoscale Res. Lett.* **2006**, *1*, 62–67.

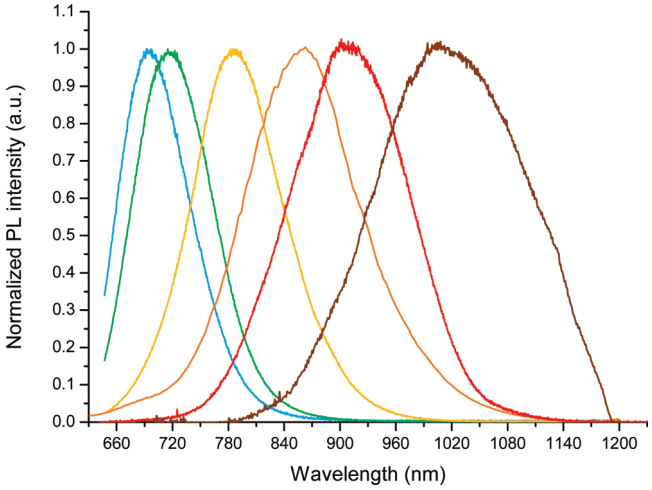

Figure 8. PL spectra of Cu−In−Se/ZnS QDs corresponding to core samples synthesized at, from left to right, T_f = 140, 160, 200, 220, and 250 °C with fast heating and 250 °C with intermediate heating. The emission maxima range from 700 nm to ~1030 nm.

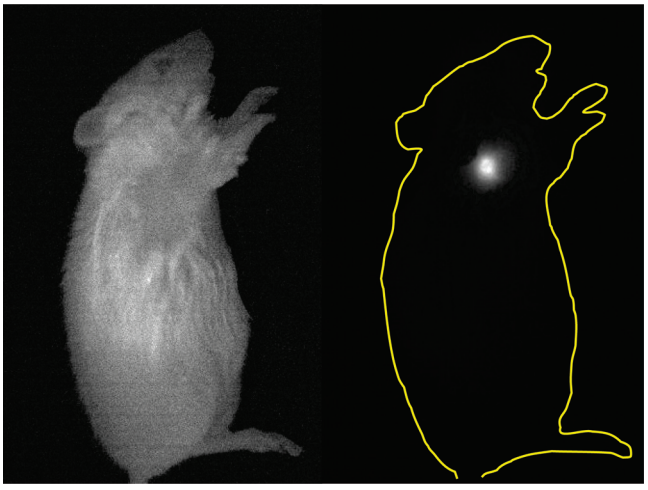

Figure 9. In vivo fluorescence imaging of the right flank of a mouse before (left) and 4 h after subcutaneous injection of QDs (right). The injection point is hidden to improve visualization of the lymph node.

fluorescence of samples emitting at visible wavelengths was detected by eye even at high temperature (200 °C) during the synthesis. This was not the case of core QDs where nonradiative recombinations from surface states prevailed. ZnS shell growth could be followed by a progressive increase in the high energy (λ < 350 nm) portion of the integrated PLE (IPLE) corresponding to the shell contribution (Figure 7). The intensity increase between 350 and 440 nm was probably due to a small diffusion of Zn into the cores. Using IPLE instead of the usual single emission wavelength PLE is preferable with broad PL spectra as it avoids selecting QD subpopulations. Final IPLE and absorption spectra were similar but showed a small amount of ZnS nanocrystals nucleation, as confirmed in XRD measurements (data not shown). Fluorescence spectra were progressively shifted to the blue (particularly for smaller cores) during shell growth, which could be due to interdiffusion of zinc into the cores. Final PL maxima covered a wide spectral range from 700 to 1030 nm (Figure 8) with ~40−50% of QY for $\lambda_{PL} \leq$ 800 nm and decreasing to ~10% for the reddest sample at ~1000 nm.

No significant growth was measured in TEM between the cores and the corresponding core/shell QDs, probably because of the small thickness of deposited ZnS compared to the size distribution (see Figure S7 in the Supporting Information). The shapes were mostly similar to the Cu−In−Se core QDs. PL measurements showed that spectral widths and decay times of core and core/shell QDs were similar (see Figure S5 in the Supporting Information), suggesting that surface passivation did not modify the nature of the emission and therefore that the defects at the origin of the PL emission are located inside the Cu−In−Se cores (data not shown).

Water solubilization of Cu−In−Se/ZnS QDs emitting at 800 nm was performed by exchanging the initial hydrophobic ligands with new hydrophilic ligands composed of a dithiol anchor group and a compact sulfobetaine zwitterionic group.[27] The exchanged QDs were stable in water and standard biological buffers for long periods of time (at least several months) and retained high quantum yields (typically 20% for PL ~ 800 nm compared to ~40% in organic solutions; this PL decrease is similar to what has been previously reported for, e.g., CdSe-based QDs[35,36]). We finally tested these core/shell QDs for *in vivo* imaging in small rodents by performing imaging of the right axillary lymph node. Lymph node status is a key prognostic factor in patients with breast cancer, because it is the first regional step of lymphatic drainage and metastasis of the primary tumor. Lymph node imaging using near-infrared fluorescent QDs may offer a promising alternative to the current procedures involving consecutive injections of radioactive colloids and blue dyes.[37,38] The QDs were purified by ultracentrifugation and ultrafiltration and ~20 μL (~0.5 optical density at 690 nm) were injected subcutaneously into the right anterior paw of healthy mice. The regional lymph node was visible as soon as a few minutes and for several hours after injection by near-infrared fluorescence imaging (Figure 9 and the Supporting Information, Figure S8), and the QD accumulation in the right axillary lymph node at 4 h postinjection corresponded to 1.42 ± 0.42% of the injected dose as indicated by ICP-MS measurements of In concentration, which is consistent with what was previously observed with other II−VI or I−III−VI_2 near-infrared QDs.[10,22,39,40] This demonstrates that the Cu−In−Se/ZnS core/shell QDs

(35) Liu, W.; Howarth, M.; Greytak, A. B.; Zheng, Y.; Nocera, D. G.; Ting, A. Y.; Bawendi, M. G. *J. Am. Chem. Soc.* **2008**, *130*, 1274–1284.
(36) Susumu, K.; Uyeda, H. T.; Medintz, I. L.; Pons, T.; Delehanty, J. B.; Mattoussi, H. *J. Am. Chem. Soc.* **2007**, *129*, 13987–13996.
(37) Ferrari, A.; Rovera, F.; Dionigi, P.; Limonta, G.; Marelli, M.; Besana Ciani, I.; Bianchi, V.; Vanoli, C.; Dionigi, R. *Expert Rev. Anticancer Ther.* **2006**, *6*, 1503–15.
(38) Rovera, F.; Frattini, F.; Marelli, M.; Corben, A. D.; Dionigi, G.; Boni, L.; Dionigi, R. *Int. J. Surg.* **2008**, *6*(Suppl 1), S109–12.
(39) Ballou, B.; Ernst, L. A.; Andreko, S.; Harper, T.; Fitzpatrick, J. A. J.; Waggoner, A. S.; Bruchez, M. P. *Bioconjugate Chem.* **2007**, *18*, 389–396.
(40) Pic, E.; Pons, T.; Bezdetnaya, L.; Leroux, A.; Guillemin, F.; Dubertret, B.; Marchal, F. *Mol. Imaging Biol.* **2009**, *12*, 394–405.
(41) Suri, D. K.; Nagpal, K. C.; Chadha, G. K. *J. Appl. Crystallogr.* **1989**, *22*, 578–583.

maintained their optical properties *in vivo* for at least several hours.

Conclusion

We have presented here a novel and simple scheme for the synthesis of fluorescent Cu−In−Se core and Cu−In−Se/ZnS core/shell QDs. This synthesis could be easily scaled up since it does not require injection or hazardous precursors. The core sizes were controlled by the final temperature of the synthesis or by the speed of the temperature rise. The resulting core−shell QDs offer PL emission tunable from 700 to 1000 nm directly dependent on the particle size, with quantum yields ranging from ~50% for smaller QDs to 10% to larger QDs in organic solvents. Their photophysical properties are consistent with donor−acceptor recombination rather than direct band edge exciton recombination. Zinc sulfide shell growth provided good PL stability in aqueous environment, as was demonstrated with *in vivo* imaging of regional lymph nodes in mice. These QDs represent a novel class of Cd-, Hg-, and Pb-free emitters in the near-infrared range up to 1 μm that extend the spectral range offered by previously reported $CuInS_2$-based QDs. Further careful studies will be needed to determine the toxicity of these Cu−In−Se/ZnS QDs, and we expect that these QDs could find numerous applications in light emitting devices or for *in vivo* imaging with reduced toxicity.

Acknowledgment. We thank X. Xu for assistance with TEM imaging. We acknowledge Agence Nationale pour la Recherche (ANR) for financial support.

Supporting Information Available: Additional experimental and methodological details (PDF). This material is available free of charge via the Internet at http://pubs.acs.org.